Geochemical Perspectives Letters

Hydrothermal vents and organic ligands sustained the Precambrian copper budget

E.E. Stüeken

Supplementary Information

The Supplementary Information includes:

- Thermodynamic Model
- Box Model
- Figures S-1 to S-7
- Tables S-1 to S-3
- Supplementary Information References

Thermodynamic Model

The thermodynamic model of mixing between hydrothermal fluid and seawater was set up in Geochemist's Workbench® (GWB, version 12.0.4), following the approach of Sander and Koschinsky (2011). The composition of the modern Rainbow hydrothermal vent field at the Mid-Atlantic Ridge was used to represent the hydrothermal endmember (Table S-1). Modern seawater (28.2 mM SO_4^{2-}, 0.7 nM Fe^{3+}) was initially equilibrated with 0.21 bar O_2 gas, resulting in 349 µM $O_{2(aq)}$. This composition was then used as a reactant in the model, *i.e.* disconnected from the atmospheric O_2 reservoir. The initial total dissolved copper (Cu_T) concentration of seawater was set to 0 in all cases. For the Proterozoic, seawater was equilibrated with 0.0021 bar O_2 (1 % present levels) (Lyons *et al.*, 2014), giving $3.5 \cdot 10^{-6}$ M $O_{2(aq)}$. This composition was then equilibrated with Fe^{2+} and SO_4^{2-} set to 100 µM (Holland, 1984) and 3 mM (Luo *et al.*, 2014), respectively. This two-step approach mimics mixing of oxygen-charged surface waters with anoxic deep waters. The final composition was anoxic (10^{-51} M $O_{2(aq)}$) and dominated by Fe^{2+} (ferruginous), consistent with observations (Planavsky *et al.*, 2011). For the Archean, Fe^{2+} was kept at 100 µM while SO_4^{2-} was set to 20 µM (Jamieson *et al.*, 2013; Crowe *et al.*, 2014). Instead of O_2, Archean seawater was equilibrated with 10^{-5} bar H_2 gas (giving $5.6 \cdot 10^{-9}$ M $H_{2(aq)}$) as suggested for the Archean atmosphere (Claire *et al.*, 2006). The final composition was thus also anoxic and ferruginous, but more reducing than in the Proterozoic. It is important to note in this context that the term ferruginous can have two different meanings: The Archean state where sulfur is stable as H_2S (though added here as SO_4^{2-}), but Fe^{2+} is relatively more abundant than H_2S, and the Proterozoic state where sulfur is present as SO_4^{2-}

while iron is stable as Fe^{2+}. The latter would have a relatively higher redox potential. To explore the sensitivity of the model, Fe^{2+} concentrations up to 1 mM were tested for the Proterozoic and Archean (Tosca *et al.*, 2016) but not found to have any significant effect on the final results (Tables S-2 and S-3). For the Proterozoic model, changing SO_4^{2-} concentrations in the range of 3-10 mM also had negligible effects (< few % difference), but decreasing SO_4^{2-} to 2 mM or less generated results more akin to the Archean. For the Archean model, lowering SO_4^{2-} to 2 µM (Crowe *et al.*, 2014) made no discernible difference while increasing it to 0.2-2 mM increased the final total Cu concentration in the hydrothermal fluid by about one order of magnitude, but this does not impact the overall conclusion of very low Archean Cu_T levels.

The hydrothermal fluid (T = 300 °C) was mixed with seawater (T = 4 °C) in proportions from 0.1 to 1000 and the fluid chemistry was monitored. To model the speciation of Cu in the presence of organic ligands, the *thermo* database in GWB was modified, following Sander and Koschinsky (2011). A hydrothermal ligand (L_h) and a seawater ligand (L_s) for Cu were added with their known dissociation constants. Also $Cu(HS)^+_{(aq)}$ and $Cu(HS)_{(aq)}$ were added as aqueous complexes (Al-Farawati and van den Berg, 1999). The initial concentration of the two ligands, based on modern observations (Sander and Koschinsky, 2011) was set to 10 nM for L_s in seawater and 0 µM, 1 µM or 10 µM for L_h in the hydrothermal fluid. Other concentrations were explored as described below. Precipitation was allowed for the following minerals: pyrite, pyrrhotite, sphalerite, galena, amorphous $Fe(OH)_3$ and $Fe(OH)_2$, birnessite, cuprite, covellite, copper, chalcopyrite, chalcocite, ferrite-Cu, malachite, azurite, barite, anhydrite, nontronite, talc and amorphous SiO_2. All major ion concentrations in the seawater endmember prior to mixing with the hydrothermal fluid were kept constant through time. The pH of the seawater endmember was varied from 6.5 in the Archean to 7.5 in the Proterozoic and 8.1 in the Phanerozoic (Halevy and Bachan, 2017; Isson and Planavsky, 2018; Krissansen-Totton *et al.*, 2018).

The REACT module of Geochemis's Workbench® was used for the thermodynamic model. The hydrothermal fluid was entered as a Basis with a total amount of 1 kg. Seawater, also 1 kg, was entered as a Reactant, and 'reactant times' was set to 1000, which allows progressive mixing of the two fluids up to a ratio of 1:1000. Under Config → Iteration, *precipitation* was turned on; all other parameters were left at their default values. Under Config → Stepping, *delxi* (the maximum allowed step in the reaction) was set to 0.0001, which allows monitoring fluid changes at lower mixing ratios. Under 'special configurations', *flow-through* and *dump* were ticked. The *dump* function forces the programme to precipitate minerals that are saturated prior to the reaction. This is a realistic scenario, because it removes saturated minerals that would naturally precipitate from a hydrothermal fluid prior to mixing with seawater. The *flow-through* function prohibits precipitated minerals to re-dissolve, which mimics settling of minerals to the seafloor, as observed in natural systems.

Box Model

Sander and Koschinsky (2011) used the end-product at a mixing ratio of 1000:1 to evaluate the imprint of hydrothermal venting on the marine Cu_T budget. However, this mixing ratio is not easily justified. In this study, the thermodynamic model was thus followed by a box model of Cu_T in the ocean, run in Stella® Professional (version 1.0.1). The box model (Fig. S-1) included a riverine (F_{river}) and a hydrothermal input flux ($F_{hydrothermal}$) of Cu in units of mol/yr. For the hydrothermal flux, the global average hydrothermal water flux of today (10^{14} L/yr) (Reinhard *et al.*, 2013) was multiplied by the total Cu concentration in mol/L obtained from the thermodynamic model at that point where precipitation had ceased. This point was chosen because it represents the moment when the mixed fluid disperses freely into the ocean without further precipitation near the vent environment. The river flux was calculated as the product of the global average river water flux ($3.74 \cdot 10^{16}$ L yr^{-1}) (Emerson and Hedges, 2008) and the average Cu concentration in rivers today ($2 \cdot 10^{-8}$ M) (Little *et al.*, 2013). For the Proterozoic, the river water flux and concentration were kept at the modern value, because oxidative weathering is thought to have started around 2.7-2.5 Ga (Stüeken *et al.*, 2012). For the Archean, the river water flux was kept constant but the riverine Cu concentration was set to 10^{-15} M (Hao *et al.*, 2017). It is likely that past river fluxes were lower when continents were smaller (Holland, 1984; Raiswell, 2006) while hydrothermal water fluxes may have been higher when the Earth was hotter.

The uncertainty bounds on these parameters are unknown and therefore not explored in detail in this model. Using a lower river water flux of $3 \cdot 10^{15}$ L yr^{-1} (Holland, 1984; Raiswell, 2006) would lower the total Cu concentration of the Proterozoic by roughly one order of magnitude (Fig. S-6), but the broad trends in Cu_T from the Archean to the modern and the relative contribution of hydrothermal Cu sources are not affected. Furthermore, the lower river flux was estimated for the Archean; in the Proterozoic when continental land mass had approached Phanerozoic levels, it is likely that the river flux was closer to the modern value. The Archean total Cu concentration does not change if the river water flux is reduced (not shown), because hydrothermal fluids by far outweigh the marine Cu budget. The sink of Cu from the ocean (F_{sink}) was modelled as a first-order reaction ($F_{sink} = V_{ocean} \cdot [Cu]_{ocean} \cdot k$) with a rate constant ($k$) equal to 1/5000 yr^{-1}, where 5000 yr is the residence time of Cu in the modern ocean (Hao *et al.*, 2017). V_{ocean} is the volume of the ocean, set equal to the modern value, and $[Cu]_{ocean}$ is the marine Cu_T concentration in mol/L. This residence time, *i.e.* the rate constant for Cu_T removal from the ocean, was varied as described below to explore the effects of Proterozoic euxinia (Lyons *et al.*, 2014). To test the relative contributions of hydrothermal and riverine Cu to the total ocean budget, the box model was run with each source flux turned on separately. The box model was run until an equilibrium value for $[Cu]_{ocean}$ was reached, which was taken as the final result.

Supplementary Figures

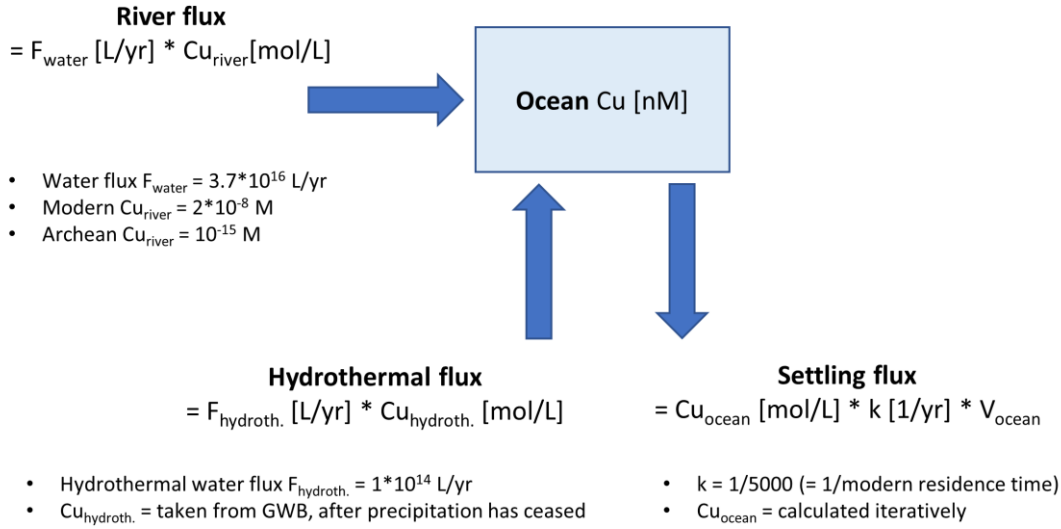

Figure S-1 Schematic of the box model run in Stella®. F_{water} = river water flux; Cu_{river} = concentration of Cu in river water; $F_{hydroth.}$ = hydrothermal water flux; $Cu_{hydroth.}$ = hydrothermal Cu concentration, taken from the thermodynamic model after precipitation has ceased; Cu_{ocean} = Cu_T concentration in seawater, i.e. target parameter of the box model; k = rate constant for Cu settling out of the ocean; V_{ocean} = total ocean volume in litres. The system was solved by integration with the Euler method.

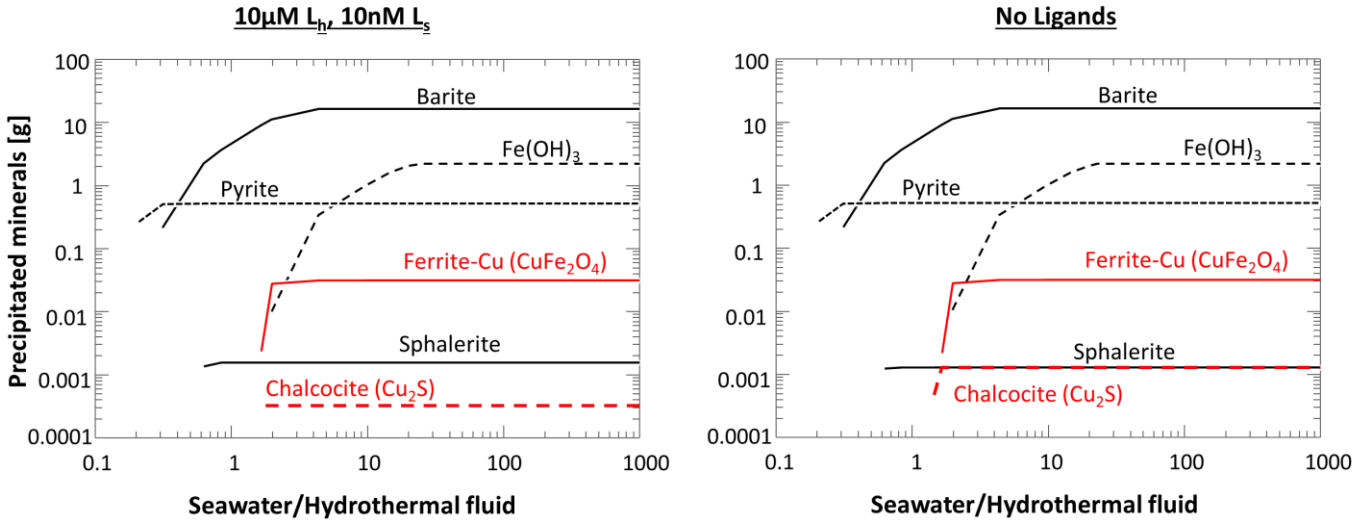

Figure S-2 Mineral precipitation in the modern ocean during mixing between 1 kg hydrothermal fluid and up to 1000 kg seawater. Copper-bearing minerals are marked in red. Note that less chalcocite is precipitated in the presence of ligands.

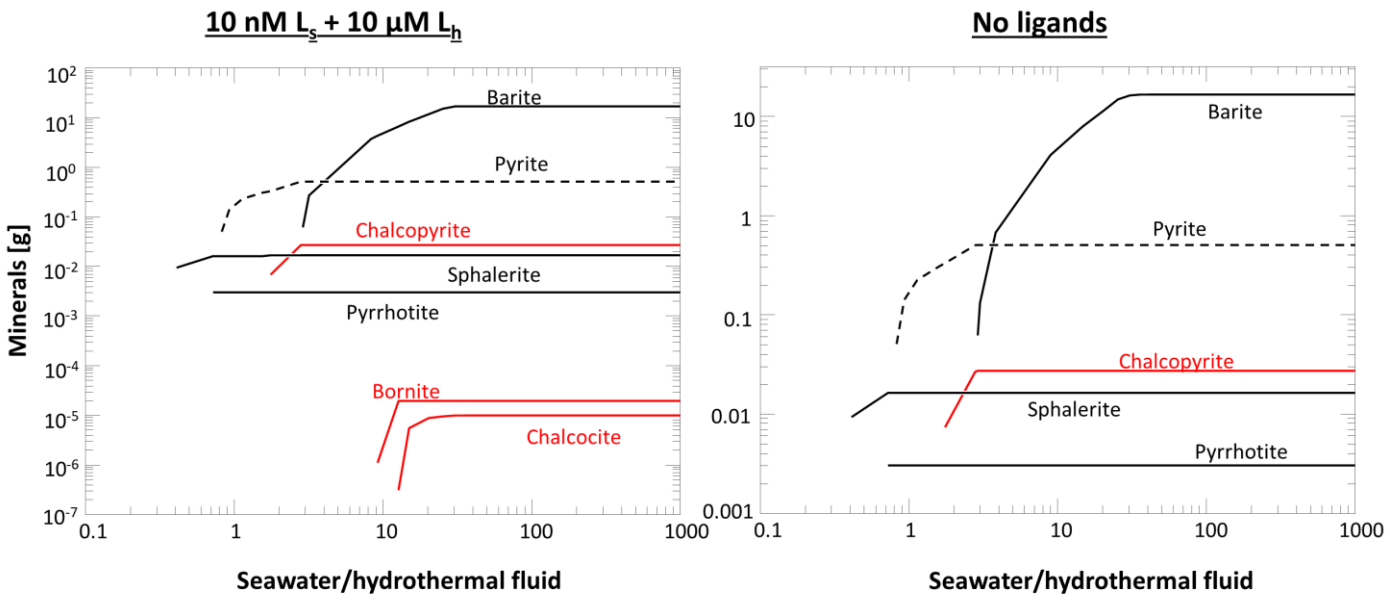

Figure S-3 Mineral precipitation in the Proterozoic ocean during mixing between 1 kg hydrothermal fluid and up to 1000 kg seawater. Copper-bearing minerals are marked in red. Less chalcopyrite is precipitated in the presence of ligands, but the difference is not visible at this scale. Note change in mineral speciation towards more Fe-depleted Cu phases (chalcocite and bornite) in the presence of ligands, which results from Cu-release from the hydrothermal ligand later during the mixing process.

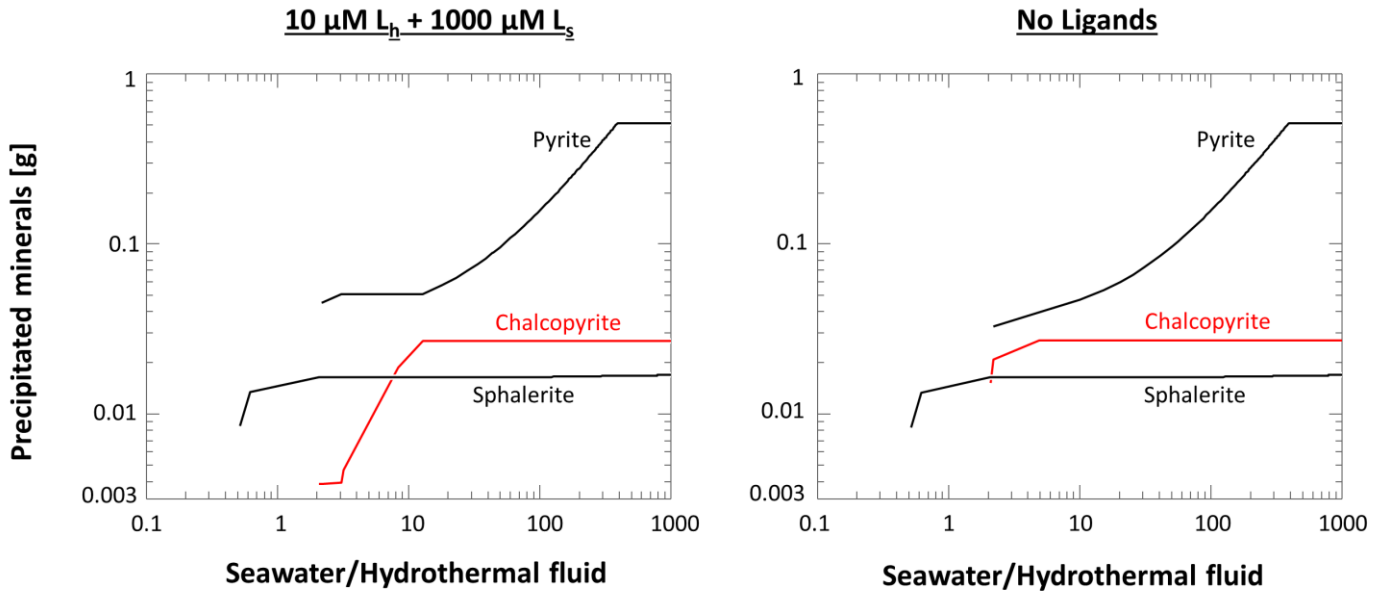

Figure S-4 Mineral precipitation in the Archean ocean during mixing between 1 kg hydrothermal fluid and up to 1000 kg seawater. Copper-bearing minerals are marked in red. Note that chalcopyrite precipitates later in the presence of ligands and overall less of it is produced.

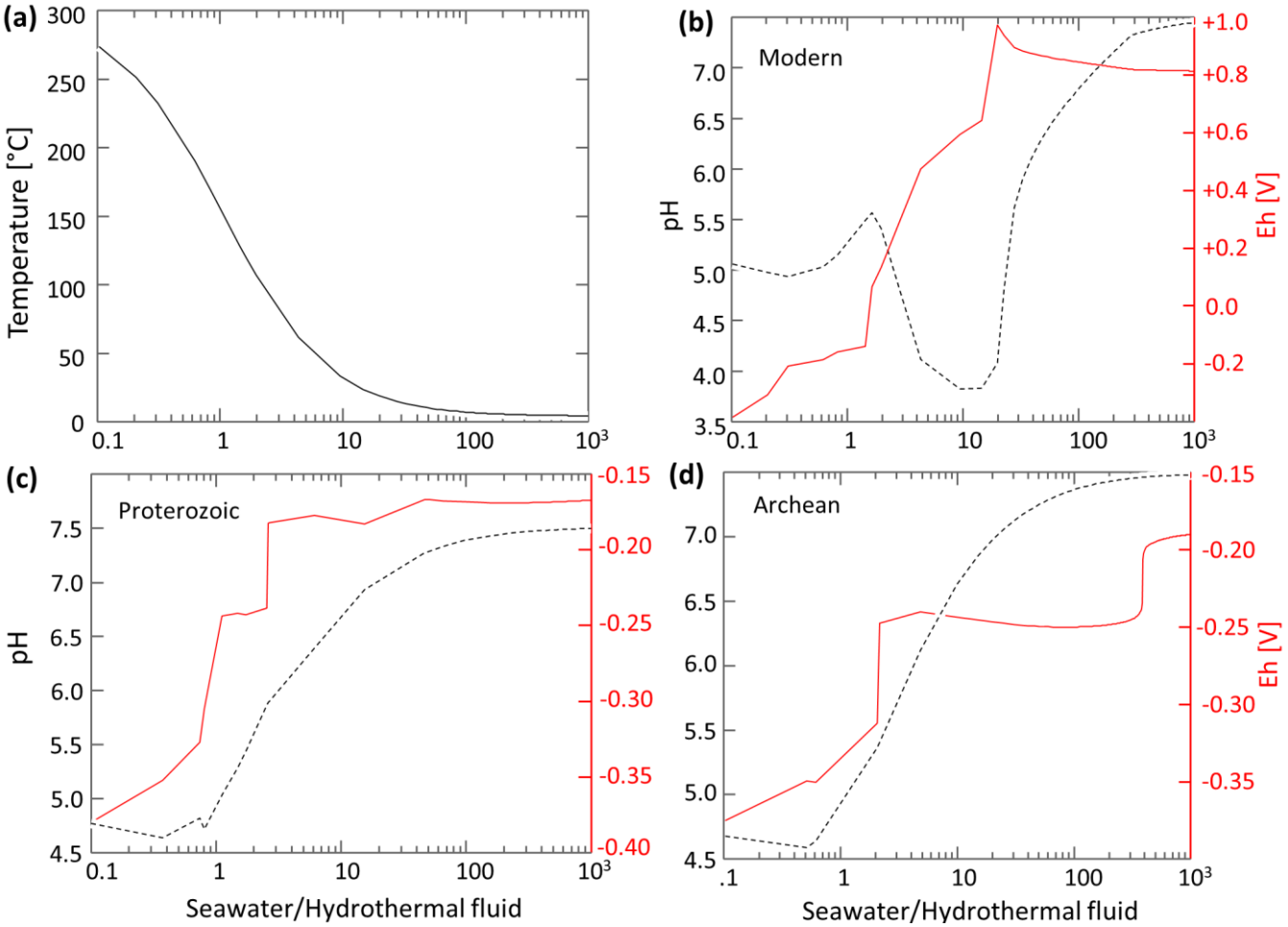

Figure S-5 Change in fluid temperature **(a)**, as well as pH and Eh for the modern **(b)**, Proterozoic **(c)** and Archean **(d)** scenario. The temperature change in panel **(a)** applies to all three time periods.

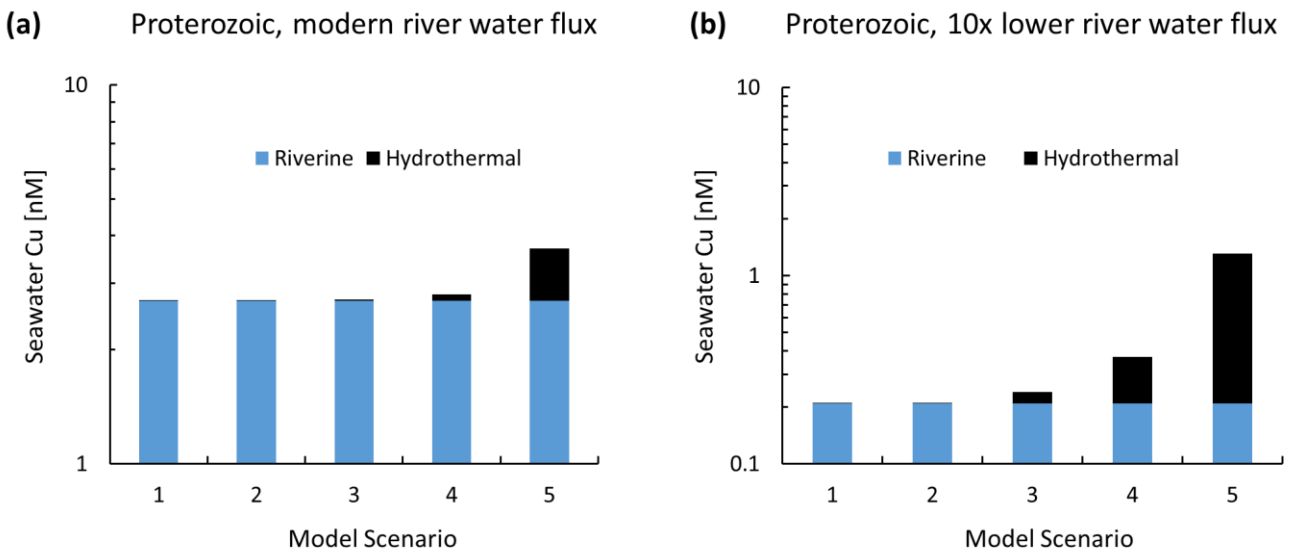

Figure S-6 Comparing the effect of different total river water fluxes on the marine Cu budget in the Proterozoic ocean. **(a)** Using the modern river water flux of $3.74 \cdot 10^{16}$ L yr^{-1} (same as Figure 1c in the main text). **(b)** Using a lower river water flux of $3 \cdot 10^{15}$ L yr^{-1}. The total marine Cu concentration in **(b)** is lower by roughly a factor of 10. However, this lower river water flux was estimated for the Archean and is therefore likely an underestimate of the Proterozoic river flux.

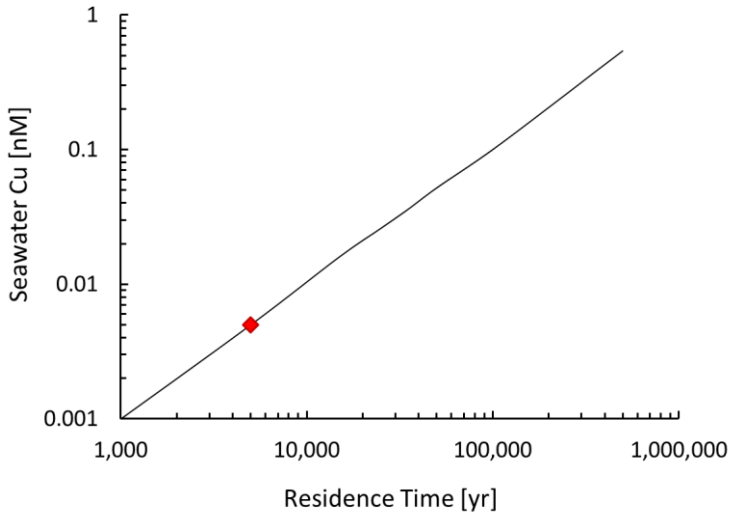

Figure S-7 Effect of increasing the total Cu residence time in the Archean ocean in a scenario with a high marine ligand (Ls) concentration of 1mM (Scenario 4 in Figure 1e in the main text). Unless ocean temperature was higher than today (Figure 1f in the main text), a longer residence time may be an alternative mechanism for maintaining nM levels of Cu_T in Archean seawater.

Supplementary Tables

Table S-1 Input data for the thermodynamic model. The hydrothermal fluid represents the Rainbow vent field in the Mid-Atlantic Ridge. Seawater constraints are described in the Methods. Note that the software requires that the two reacting fluids contain all constituents. Therefore, L_h and L_s had to be added also the seawater and the hydrothermal fluid, respectively, but their concentrations were set to extremely low values (10^{-20}), which are essentially zero for practical purposes.

Hydrothermal fluid			Modern seawater			Proterozoic seawater			Archean seawater		
Ba^{2+}	67	uM	Ba^{2+}	$9.21\cdot10^{-8}$	M	Ba^{2+}	$9.21\cdot10^{-8}$	M	Ba^{2+}	$9.21\cdot10^{-8}$	M
Ca^{2+}	67	mM	Ca^{2+}	$1.07\cdot10^{-2}$	M	Ca^{2+}	$1.07\cdot10^{-2}$	M	Ca^{2+}	$1.07\cdot10^{-2}$	M
Cl^-	750	mM	Cl^-	$5.91\cdot10^{-1}$	M	Cl^-	$5.91\cdot10^{-1}$	M	Cl^-	$5.91\cdot10^{-1}$	M
Cu^+	140	uM	Cu^+	$7.26\cdot10^{-9}$	nM	Cu^+	$7.26\cdot10^{-9}$	nM	Cu^+	$7.26\cdot10^{-9}$	nM
Fe^{2+}	24000	uM	Fe^{2+}	$1\cdot10^{-9}$	M	Fe^{2+}	100	uM	Fe^{2+}	100	uM
K^+	20	mM	K^+	$1.05\cdot10^{-2}$	M	K^+	$1.05\cdot10^{-2}$	M	K^+	$1.05\cdot10^{-2}$	M
L_h^-	10	uM	L_h^-	$1\cdot10^{-20}$	nM	L_h^-	$1\cdot10^{-20}$	nM	L_h^-	$1\cdot10^{-20}$	nM
L_s^-	$1\cdot10^{-20}$	nM	L_s^-	10	nM	L_s^-	10	nM	L_s^-	10	nM
Mg^{2+}	0.0001	nM	Mg^{2+}	$5.66\cdot10^{-2}$	M	Mg^{2+}	$5.66\cdot10^{-2}$	M	Mg^{2+}	$5.66\cdot10^{-2}$	M
Mn^{2+}	2250	uM	Mn^{2+}	$1\cdot10^{-9}$	M	Mn^{2+}	$1\cdot10^{-9}$	M	Mn^{2+}	$1\cdot10^{-9}$	M
Na^+	553	mM	Na^+	$5.06\cdot10^{-1}$	M	Na^+	$5.06\cdot10^{-1}$	M	Na^+	$5.06\cdot10^{-1}$	M
$SiO_{2(aq)}$	6.9	mM	$SiO_{2(aq)}$	$1.70\cdot10^{-4}$	M	$SiO_{2(aq)}$	$1.70\cdot10^{-4}$	M	$SiO_{2(aq)}$	$1.70\cdot10^{-4}$	M
Sr^{2+}	200	uM	Sr^{2+}	$1.33\cdot10^{-5}$	M	Sr^{2+}	$1.33\cdot10^{-5}$	M	Sr^{2+}	$1.33\cdot10^{-5}$	M
Zn^{2+}	160	uM	Zn^{2+}	$1.04\cdot10^{-8}$	M	Zn^{2+}	$1.04\cdot10^{-8}$	M	Zn^{2+}	$1.04\cdot10^{-8}$	M
$CH_{4(aq)}$	2.5	mM	HCO_3^-	$2.06\cdot10^{-3}$	M	HCO_3^-	$2.06^{-}\cdot10^{3}$	M	HCO_3^-	$2.06\cdot10^{-3}$	M
H_2S	1	mM	SO_4^{2-}	28	mM	SO_4^{2-}	$3\cdot10^{-3}$	M	SO_4^{2-}	20	uM
$H_{2(aq)}$	16	mM	$O_{2(aq)}$	349	uM	$O_{2(aq)}$	$3.49\cdot10^{-51}$	M	$H_{2(aq)}$	$7.90\cdot10^{-9}$	M
pH	4.8		pH	8.1		pH	7.5		pH	6.5	
T	300	°C	T	4	°C	T	4	°C	T	4	°C

Table S-2 Changing SO_4^{2-} or Fe^{2+} in the Proterozoic ocean. These tests represent the scenario with 10 µM L_h^+ and 10 nM L_s^+. The second column shows the concentration of residual Cu in the fluid mixture after precipitation has ceased. Note the sudden decline in Cu levels when sulfate levels drop to 2 mM. 'Used' indicates the value that was used for the model in the main text.

Seawater SO_4^{2-} [mM]	**Final hydrothermal vent Cu [M]**
2	$4.8 \cdot 10^{-11}$
3 (used)	$2.0 \cdot 10^{-9}$
4	$1.5 \cdot 10^{-9}$
5	$1.37 \cdot 10^{-9}$
10	$1.36 \cdot 10^{-9}$
Seawater Fe^{2+} [uM]	**Final hydrothermal vent Cu [M]**
100 (used)	$2.0 \cdot 10^{-9}$
1000	$1.83 \cdot 10^{-9}$

Table S-3 Changing SO_4^{2-} or Fe^{2+} in the Archean ocean. These tests represent the scenario with 10 µM L_h^+ and 10 nM L_s^+. Residual Cu in the fluid more than doubles with increasing sulfate, but sulfate concentrations above 200 µM are probably unrealistic for the Archean ocean. 'Used' indicates the value that was used for the model in the main text.

Seawater SO_4^{2-} [µM]	**Final hydrothermal vent Cu [M]**
2	$4.28 \cdot 10^{-12}$
20 (used)	$4.50 \cdot 10^{-12}$
200	$1.36 \cdot 10^{-11}$
2000	$1.63 \cdot 10^{-11}$
Seawater Fe^{2+} [uM]	**Final hydrothermal vent Cu [M]**
100 (used)	$4.50 \cdot 10^{-12}$
1000	$2.30 \cdot 10^{-12}$

Supplementary Information References

Al-Farawati, R., van den Berg, C.M. (1999) Metal–sulfide complexation in seawater. *Marine Chemistry* 63, 331-352.

Claire M.W., Catling D.C., Zahnle K.J. (2006) Biogeochemical modelling of the rise in atmospheric oxygen. *Geobiology* 4, 239-269.

Crowe, S.A., Paris, G., Katsev, S., Jones, C., Kim, S.T., Zerkle, A.L., Nomosatryo S., Fowle D., Adkins J.F., Sessions A.L., Farquhar J., Canfield D.E. (2014) Sulfate was a trace constituent of Archean seawater. *Science* 346, 735-739.

Emerson, S., Hedges, J. (2008) *Chemical oceanography and the marine carbon cycle.* Cambridge University Press, Cambridge, UK.

Halevy, I., Bachan, A. (2017) The geologic history of seawater pH. *Science* 355, 1069-1071.

Hao, J., Sverjensky, D.A., Hazen, R.M. (2017) Mobility of nutrients and trace metals during weathering in the late Archean. *Earth and Planetary Science Letters* 471, 148-159.

Holland, H.D. (1984) *The chemical evolution of the atmosphere and oceans,* Princeton University Press, Princeton, NJ.

Isson, T.T., Planavsky, N.J. (2018) Reverse weathering as a long-term stabilizer of marine pH and planetary climate. *Nature* 560, 471-475.

Jamieson, J.W., Wing, B.A., Farquhar, J., Hannington, M. (2013) Neoarchaean seawater sulphate concentrations from sulphur isotopes in massive sulphide ore. *Nature Geoscience* 6, 61-64.

Krissansen-Totton, J., Arney, G.N., Catling, D.C. (2018) Constraining the climate and ocean pH of the early Earth with a geological carbon cycle model. *Proceedings of the National Academy of Sciences* 115, 4105-4110.

Little, S.H., Vance, D., Walker-Brown, C., Landing, W.M. (2013) The oceanic mass balance of copper and zinc isotopes, investigated by analysis of their inputs, and outputs to ferromanganese oxide sediments. *Geochimica et Cosmochimica Acta* in press.

Luo, G., Ono, S., Huang, J., Algeo, T.J., Li, C., Zhou, L., Robinson, A., Lyons, T.W., Xie, S. (2014) Decline in oceanic sulfate levels during the early Mesoproterozoic. *Precambrian Research* 258, 36-47.

Lyons, T.W., Reinhard, C.T., Planavsky, N.J. (2014) The rise of oxygen in Earth's early ocean and atmosphere. *Nature* 506, 307-315.

Planavsky, N.J., McGoldrick, P., Scott, C.T., Li, C., Reinhard, C.T., Kelly, A.E., Chu, X., Bekker, A., Love, G.D., Lyons, T.W. (2011) Widespread iron-rich conditions in the mid-Proterozoic ocean. *Nature* 477, 448-451.

Raiswell, R. (2006) An evaluation ofdiagenetic recycling as a source of iron for banded iron formations. In: Kesler, S.E., Ohmoto, H. (Eds.) *Evolution of Early Earth's Atmosphere, Hydrosphere, and Biosphere: Constraints from Ore Deposits.* Geological Society of America Memoir, Boulder, Colorado, 223-238.

Reinhard, C.T., Planavsky, N.J., Robbins, L.J., Partin, C.A., Gill, B.C., Lalonde, S.V., Bekker, A., Konhauser, K.O., Lyons, T.W. (2013) Proterozoic ocean redox and biogeochemical stasis. *Proceedings of the National Academy of Sciences* 110, 5357-5362.

Sander, S.G., Koschinsky, A. (2011) Metal flux from hydrothermal vents increased by organic complexation. *Nature Geoscience* 4, 145-150.

Stüeken, E.E., Catling, D.C., Buick, R. (2012) Contributions to late Archaean sulphur cycling by life on land. *Nature Geoscience* 5, 722-725.

Tosca, N.J., Guggenheim, S., Pufahl, P.K. (2016) An authigenic origin for Precambrian greenalite: Implications for iron formation and the chemistry of ancient seawater. *GSA Bulletin* 128, 511-530.